Numerical Simulations on Performance of a Hybrid and a Tandem Rotor

Shubhali More, Amit Kumar, and A. M. Pradeep

Abstract In the quest of maximizing the pressure ratio and the efficiency of the gas turbine engine, designing a compressor that can generate the required pressure ratio with a minimum number of stages is one of the challenges. A single blade, if designed with a higher diffusion factor, has an inherent problem of flow separation. Tandem or slotted blades with the help of nozzle-gap phenomenon have shown promising results in terms of higher pressure ratio and efficiency, but it has mechanical complexity and lower stall margin. The hybrid rotor called part-span tandem has been designed to get the benefits of both a single rotor as well as tandem rotor blades. Design methodology as well as parallel comparison of results of a low speed hybrid rotor, tandem rotor, and a single rotor is included in the paper. CFD results such as pressure distribution at different span locations, total pressure rise, static pressure rise, contours of Mach number, entropy, the behavior of the tip leakage flow, and performance curve are included in this paper. Full span tandem rotor has higher pressure rise, and the hybrid rotor has a better stall characteristic.

Nomenclatures

Cp	Static pressure coefficient $= P - P_{\text{in}}/0.5\rho U_{\text{tip}}^2$
$\dot{m}$	Mass flow rate (kg/s)
P	Static pressure (Pa)
$P0$	Total pressure (Pa)
t/s	Tandem percentage pitch
U	Tangential speed of rotor (m/s)
$\Delta X1/\Delta X2$	Tandem overlap in the axial direction
Z/H	Span percentage

S. More (✉) · A. Kumar · A. M. Pradeep
Indian Institute of Technology Bombay, Mumbai, Maharashtra 400076, India
e-mail: shubhalimore182@gmail.com

A. M. Pradeep
e-mail: ampradeep@aero.iitb.ac.in

G. Sivaramakrishna et al. (eds.), *Proceedings of the National Aerospace Propulsion Conference*, Lecture Notes in Mechanical Engineering,
https://doi.org/10.1007/978-981-19-2378-4_2

Greek Symbols

φ	Flow coefficient $= C_a/U_m$
$k-\varepsilon$	K-Epsilon turbulence model
ρ	Density (kg/m^3)
ω	Total pressure loss coefficient $= \frac{(P_{0\_rel\_LE} - P_{0\_rel\_TE})}{0.5 * \rho * U_{tip}^2}$
ψ	Stagnation total pressure rise coefficient $= (P0 - P0_{in})/0.5\rho U_m^2$

Subscript

ex	Exit location
in	Inlet location
m	Mean section
rel	Relative frame of reference
x	Variable location
tip	Tip section

Abbreviations

AB	Aft blade
AO	Axial overlap
CDA	Control diffusion airfoil
DCA	Double circular airfoil
DF	Diffusion factor
DR	Degree of reaction
FB	Forward blade
LE	Leading edge
PP	Percentage pitch
PS	Pressure side
SS	Suction side
SST	Shear stress turbulence model
TE	Trailing edge
TLV	Tip leakage vortex

1 Introduction

A gas turbine designer's aim is for higher specific thrust and lower fuel consumption. Compressors occupy a larger section in the gas turbine engine. A compressor blade with higher diffusion capability can significantly contribute to lowering the engine weight and therefore making it more compact. However, the maximum diffusion factor and flow turning angle has a limit because of the adverse pressure gradient and flow separation.

Due to the high turning angle of a single blade, flow near to the trailing edge (TE) on the suction side (SS) of the blade leads to separation. In the tandem blade, a single blade airfoil is divided into two airfoils to form a separate forward blade (FB) and aft blade (AB) as shown in Fig. 1. A nozzle like a gap is formed between these two tandem blades. Due to the pressure difference near the gap nozzle, the flow from the pressure side (PS) of FB passes through the gap nozzle and provides an extra source of energy to the sluggish flow over the suction surface of the aft blade. Due to extra momentum transfer, flow separation can be effectively delayed. As the diffusion factor (DF) limit increases, pressure rises per stage, and blade loading capacity increases and hence improvement in overall performance characteristics.

But Saha and Roy [1] have noted down tandem is less effective as compared to baseline in a low diffusion region (camber angle less than 40° region), as the nozzle gap is less efficient due to available low momentum of the fluid and also flow complexities at the tip region which increases because of tip leakage vortex (TLV) phenomenon. In the tandem rotor, the numbers of blades are more compared to a single rotor blade which increases the total tolerance requirement. The hybrid rotor is designed to get the benefit of higher pressure rise along with the efficiency of the

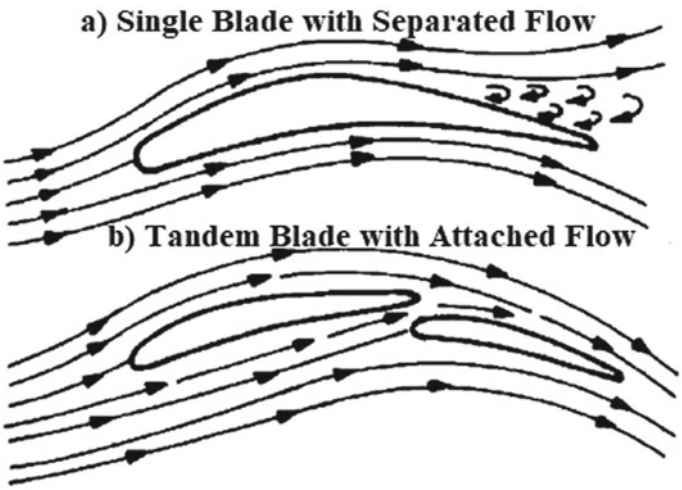

Fig. 1 Fundamental of tandem blade

tandem rotor as well as the better stall margin and design simplicity of the single rotor. The part-span tandem rotor is a mixed combination of tandem airfoils in high diffusion region and single airfoils in low diffusion regions and both are stacked together to form a hybrid rotor blade.

Saha and Roy [1] experimentally analyzed that tandem airfoil blade CDA (Control Diffusion Airfoil) 32–21 which has extra 5° camber results in more turning of flow without separation than tandem airfoil CDA 21–21 and single airfoil blade CDA 43. Kumar and Pradeep [2] have noted from the numerical investigation that tandem shows a 3.6% increase in a total pressure rise and a 2.3% increase in efficiency than a single rotor stage at the design point. Also, it is found that at off-design condition, tip leakage losses are lower at the tip of AB than the tip of FB at the design condition. McGlumphy [3] and McGlumphy et al. [4] done numerical investigation using RANS and Baldwin–Lomax turbulence model on tandem airfoil NACA-65 in the low speed region and analyzed results with the varying AO (Axial Overlap) and PP (percentage pitch) parameter. Noted that optimum choice for the design of tandem considering aerodynamic parameters and mechanical limitations into account was tandem with 0% AO and 85% PP. Kumar and Pradeep [5] performed high fidelity optimization numerical study and concluded that if there is significant variation in stagger and camber, then the optimized value of AO and PP at one section may or may not be optimum at other sections. Guochuan et al. [6] tested experimentally the different Double Circular Arc (DCA) profile type tandem airfoil with camber, stagger, AO, and PP as a design variable and reported for optimum results. The values of AO and PP combination differ based on the application of the blade. It is also noted that the blade chord ratio in the range of 0.6–1.0 will give optimized results. Falla's [7] computational study using RANS and $k-\omega$ turbulence model on a NACA-65 tandem airfoil reported that low AO and high PP gave suitable results for tandem configuration. McGlumphy [3], McGlumphy et al. [4], Roy, and Saha [8], Bammert, and Beelte [9] and Roy et al. [10] had primarily focused their investigations on the tandem stator or tandem cascade and have found that compared to a single blade, the tandem blade has a higher diffusion capability. In some limited literature, Hasegawa [11], Bammert, and Beelte [9] investigated the tandem rotor for a stage.

Roy et al. [10] has noted down the limitation of the tandem blade and presented the concept of a hybrid blade. It is also noted that the performance of the tandem blade depends more on the tangential gap than the axial gap. Results are superior to single airfoil if the gap is optimized. Yoon et al. [12] used RANS with SST $k-\omega$ turbulence model and demonstrated that for a given flow rate but with the slot, a minor change in the efficiency and total pressure ratio can be achieved. It also concluded that to enhance the stall margin slot is a better option than increasing tip clearance.

2 Experimental Setup

Experiments are carried out on the compressor test rig schematic of which is shown in Fig. 2, in the turbo-machinery laboratory of the IIT, Bombay. The hub and a tip

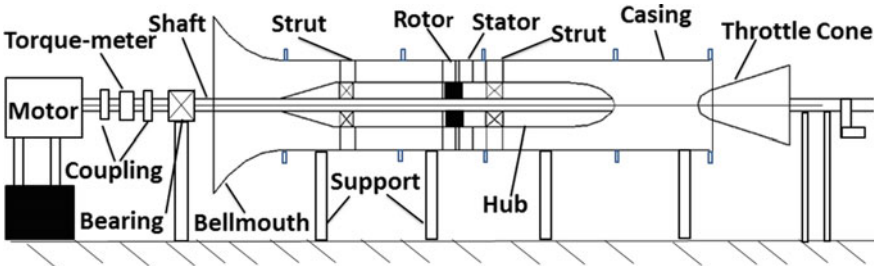

Fig. 2 Schematic of a single-stage compressor test rig

diameter of the test rig are 250 mm and 500 mm, respectively. It is specially designed for low speed applications. Mass flow variation at the outlet is achieved with the help of an automated throttle mechanism. The positions of total pressure and Kiel probes are depicted in Fig. 3. Pitot static rakes have been placed at 1.5C ahead of the leading edge (LE) of the rotor, while 4 Kiel pressure rakes are circumferentially placed at 0.5C downstream of TE of the stator. Based on experimental data, a performance map can be plotted.

The baseline stage comprised 19 rotor blades and 21 stator blades. A constant tip clearance of 1 mm is maintained for rotor blades. Owing to the low speed application, the C4 type of airfoil is used for both rotor and stator blades. The design RPM of the rotor blade is 2700, whereas the design mass flow rate is 6 kg/s. The aspect ratio of the designed blade is 1.5. The design parameters of the baseline stage are listed in Tables 1 and 2.

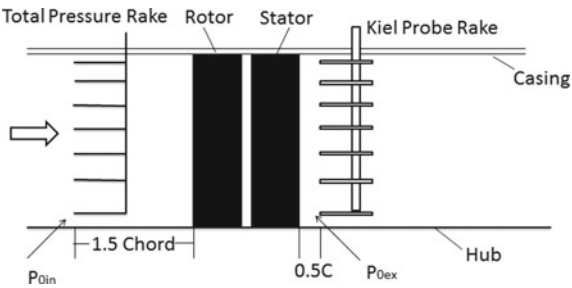

Fig. 3 Schematic of probe position

Table 1 Single rotor design specification

Rotor	Tip	Mean	Hub
DF	0.5	0.54	0.47
DR	0.78	0.70	0.50
Camber	23°	35°	60°

Table 2 Single stator design specification

Rotor	Tip	Mean	Hub
DF	0.53	0.48	0.45
Camber	50.0°	50.0°	52.0°

3 CFD Validation

For the validation purpose, the experimental data are compared with the CFD results of the baseline stage. A steady RANS simulation is carried out with two different turbulence models, namely Shear Stress Turbulence (SST) and K-Epsilon ($k-\varepsilon$). The total pressure coefficient (Ψ) is plotted with the flow coefficient (φ) and depicted in Fig. 4. SST model demonstrates better matching with the experimental data than the $k-\varepsilon$ model. At the design point, the maximum deviation in the prediction of the SST model from experimental data is 1.3%. $k-\varepsilon$ model largely under predict the total pressure value at a higher mass flow rate. At a lower mass flow rate, a slight over-prediction is observed for the $k-\varepsilon$ model. At the design point, the deviation between the $k-\varepsilon$ model than the experimental value is 7.5%. Hence, further CFD analysis is carried out with the SST turbulence model.

The paper compares the performance of the single rotor, tandem rotor, and hybrid rotor. All three rotors are designed for equal pressure rise. The total pressure distribution along the blade span is kept the same for all three blades. Design specifications of the single rotor given in Table 3. Works of the literature suggest a higher PP and lower AO tandem configuration as an optimum design configuration. Kumar and

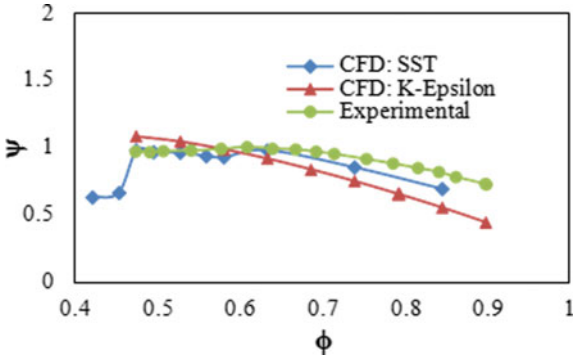

Fig. 4 Performance map of baseline stage

Table 3 Design details of the single rotor

Rotor	Tip	Mean	Hub
DF	0.63	0.62	0.48
Camber	33.0°	48.0°	66.0°
Stagger	49.0°	33.0°	10.0°

Table 4 Design specifications of the forward and aft blade of tandem

Rotor	Forward blade			Aft blade		
	Tip	Mean	Hub	Tip	Mean	Hub
DF	0.44	0.46	0.44	0.52	0.49	0.31
Camber	16.5°	20.6°	30.9°	26.1°	35.3°	42.6°
Stagger	57.5°	46.4°	28.1°	45.1°	26.6°	0.6°

Pradeep [5] selected a tandem rotor, with 5% AO and 85% PP, for their CFD analysis. The same tandem rotor is taken as a reference for the design of a hybrid rotor. The design details of the tandem forward and the aft rotor are listed in Table 4.

The single rotor blade serves as a baseline for CAD model of the hybrid rotor blade. At mid-span, a nozzle type of slot is made till a mid-section of the blade. While doing so, a single airfoil is split into two airfoils. A constant nozzle shape is maintained till mid-section airfoil. To facilitate the smooth flow in this region, the LE portion of AB has been slightly modified. From hub to mid-span, the blade has two airfoils, while from mid-span to tip, the blade has a single airfoil. Figure 5 shows two airfoils and the gap nozzle of the hybrid blade. Because of stagger angle, AO changes from hub to tip but gap shape and length of the nozzle are constants till mid-span. Table 5 contains design parameters used for the hybrid blade. The reader should understand the difference between a tandem rotor blade and a hybrid rotor. In the tandem rotor, both forward and aft rotor blade have designed separately but they are arranged in a manner that a nozzle type shape is formed in between. The exit angle of the FB serves as an inlet angle for the AB. On the contrary, the geometry of the hybrid blade is obtained by making a nozzle type slot in a single rotor design. Unlike the tandem rotor, the radius of the trailing edge of the forward airfoil and the leading edge of the aft airfoil are not pre-defined.

In-build Design Modular and Mesh of ANSYS WORKBENCH used to prepare unstructured mesh. A steady RANS (Reynolds-Averaged Navier–Stokes) equation with the SST turbulence model is used for analysis, and the numerical investigation

Fig. 5 Nozzle gap of hybrid blade

Table 5 Geometric parameters of hybrid blade

Aspect ratio	1.5
Axial overlap at mid (%)	2.80
Axial overlap at hub (%)	4.37

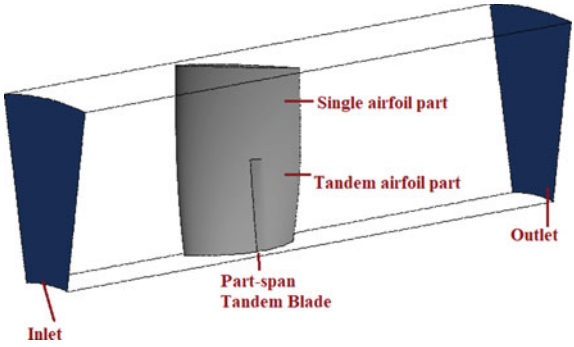

Fig. 6 Computational domain of hybrid rotor

is done with the help of ANSYS CFX solver. Figure 6 shows the CFD domain used for the numerical study. Inlet is at upstream of rotor LE by 1.5 times of airfoil chord, and outlet is at downstream of rotor TE by a distance of 2.5 times of chord. Ambient pressure at inlet and mass flow rate at the outlet are implemented as a boundary condition of the domain. After grid independence study, 2.2 million, 1.8 million, and 2.1 million mesh elements were selected for performance analysis of single, tandem, and hybrid blades, respectively, with considering wall $y+$ and quality of the mesh.

4 Results and Discussion

CFD results were extracted and analyzed at the design point $\phi = 0.64$, and off-design/near stall condition, $\phi = 0.61$. Contours of Mach number with streamlines are extracted at the three different span locations (Z/H) (10, 50, and 90%) for the single rotor, tandem rotor, and the hybrid rotor. Figures 7 and 8 shows the Mach number contours of the single rotor under design and off-design condition. Near the design point, the low velocity zone is visible near the trailing edge portion of the single rotor. However, at a 50% span, streamlines indicate reverse flow near the trailing edge of the rotor suction surface. At other span locations, flow is attached to the blade surface and flow reversal is not seen. Under the off-design condition, the

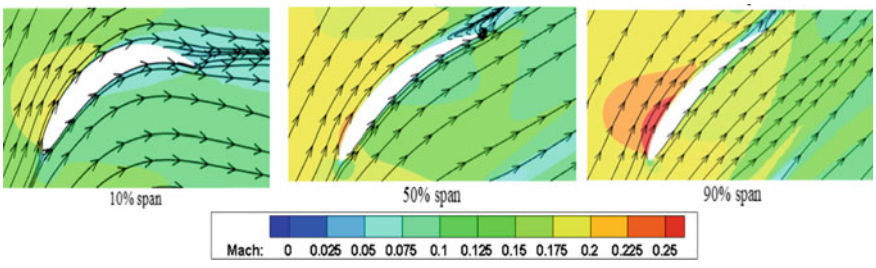

Fig. 7 Mach contours of single rotor at $\phi = 0.64$

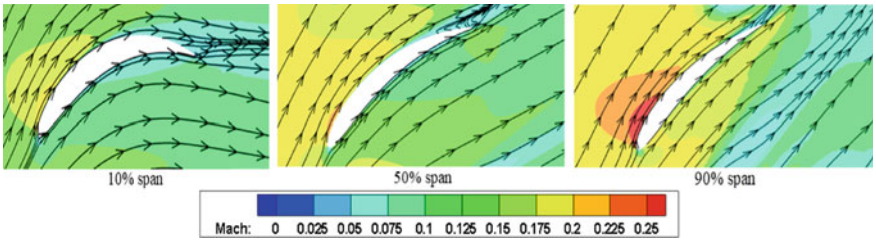

Fig. 8 Mach contours of single rotor at $\phi = 0.61$

performance of the single rotor further deteriorates and a low velocity zone enlarges further. On the contrary, the tandem rotor exhibits improved performance under design and off-design conditions (Figs. 9 and 10). Nozzle gap plays an important role in the performance of the tandem rotor. Momentum transfer through the gap is less effective near to the hub region as compared to the tip region. The lower momentum toward the hub region is mainly attributed to two factors. Firstly, the tandem rotor is designed with a low hub to tip ratio, and less energy available toward the lower span adversely affects the performance of the tandem rotor. Secondly, the pressure difference in the vicinity of the gap nozzle acts as a driving force the momentum transfer through the gap nozzle. As the pressure gradient is significantly higher toward the tip region, improved performance of the tandem rotor is observed under design and off-design condition. With less flow velocity and higher incidence,

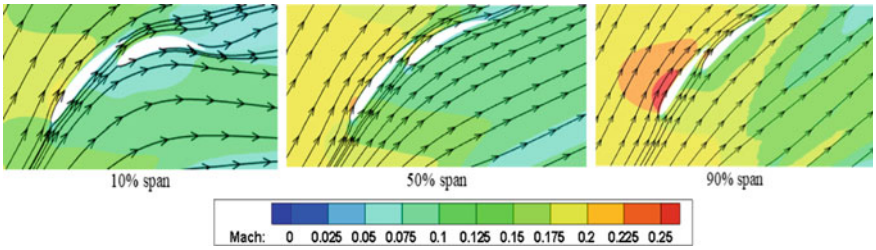

Fig. 9 Mach contours of tandem rotor at $\phi = 0.64$

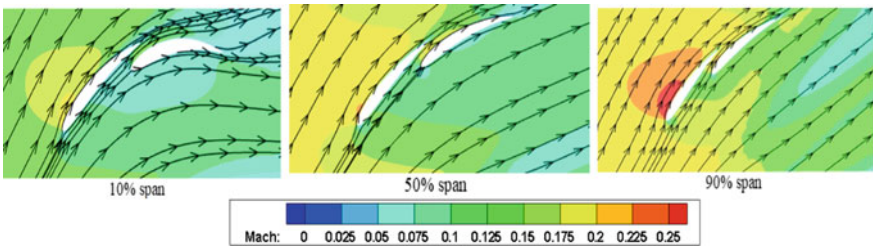

Fig. 10 Mach contours of tandem rotor at $\phi = 0.61$

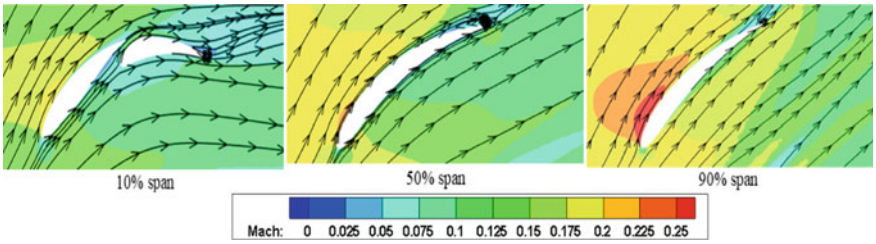

Fig. 11 Mach contours of hybrid rotor at $\phi = 0.64$

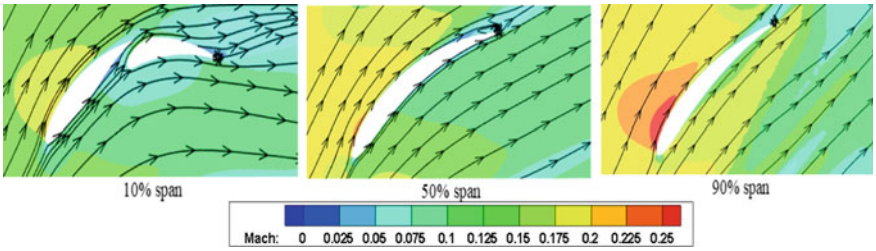

Fig. 12 Mach contours of hybrid rotor at $\phi = 0.61$

the effectiveness of the gap decreases under the off-design condition. At all spans, due to effective and optimum nozzle effect, tandem shows a lesser low velocity zone on SS of blade surface near to TE as compared to a single rotor (Figs. 11 and 12). The flow separation, which was visible in the case of a single rotor, is effectively mitigated with the help of higher momentum fluid. Mach number contours of the hybrid rotor are shown by Figs. 11 and 12. Similar to the tandem rotor case, a nozzle type shape forms in case of hybrid rotor at a lower span. The shape and size of the nozzle of hybrid rotor is different from that of the tandem rotor. At 10% span location, streamlines are attached to the AB surface under design and off-design condition. Similar to earlier cases, low velocity zones are visible near the trailing edge of the rotor blade. In the case of the hybrid rotor, aft section airfoil is too close to the pressure surface of the forward airfoil, which alters the pressure distribution pattern in that vicinity. At 50% span location, hybrid rotor shows a relatively enlarged portion of low velocity fluid. At mid-span, a transformation from tandem airfoil to a single airfoil takes place. Therefore, additional losses occur at the interface for the hybrid rotor. At the off-design conditions, the low velocity region on the blade surface has slightly moved further upstream and enlarged. The effect of TLV can be seen at a 90% span location, where a large low velocity zone is visible in the blade passage. In the case of a hybrid rotor, redesigning the nozzle gap for optimum AO can enhance the momentum transfer.

The static pressure coefficient (Cp) at various spanwise locations of the blade is shown in Figs. 13 and 14 for design and off-design condition, respectively. Blade loading increases from the hub toward the tip, and it is as per the design of single

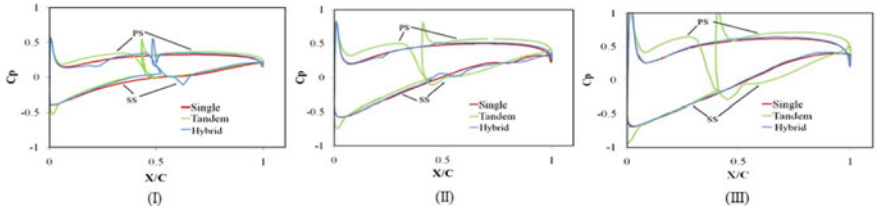

Fig. 13 Pressure coefficient (Cp) distribution at design condition (I) 10% span (II) 50% span (III) 90% span

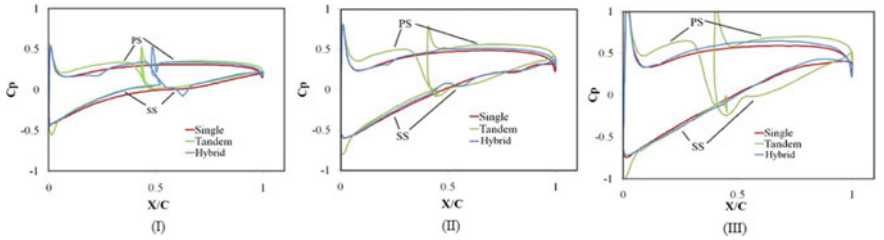

Fig. 14 Pressure coefficient (Cp) distribution at off-design condition (I) 10% span (II) 50% span (III) 90% span

and tandem rotors. Blade loading is nearly the same for all the cases at 10% span location. As the hybrid rotor is a modification of a single rotor, thus both hybrid rotor and single rotor demonstrates approximately equal blade loading, except at lower spans, where a small difference in Cp can be seen due to LE curvature of AB. Quick acceleration over aft airfoil results in a drop in Cp on SS at ~0.62 X/C. In the case of the tandem rotor, momentum transferred through gap nozzle increases the acceleration over SS of AB, which is reflected as higher negative Cp and improved blade loading. Accelerated flow over AB is due to the shape of AB and momentum transfer from the gap nozzle. The effect of gap nozzle in the tandem case is seen more clearly at 50 and 90% of the span.

As per the design, the tip section is designed for higher pressure rise. However, with the help of the nozzle-gap effect, a continuous diffusion is achieved near the tip section in the case of the tandem rotor. Clearly, the blade section is designed with a higher diffusion factor, the tandem rotor demonstrates its superiority over the single rotor. The position of AB increases the loading on the PS of FB. As TE of FB comes under the stagnation portion of AB, it increases pressure over PS of FB. The single rotor has a flatter distribution of Cp on SS, which shows less diffusivity of the blade. As a design and off-design points are close enough, there is no much variation in the nature of plots. Relatively, the tandem has higher diffusion at 50 and 90% span up to TE of the rotor. Due to the nozzle gap, higher turning capability developed in tandem, and hence, higher static pressure rise achieved.

A significant portion of losses occurs in the turbo-machinery are associated with TLV. Hence, it is important to analyze the behavior of TLV of new designs. The

formation and propagation of TLV inside the blade passage are shown with the help of entropy contours, which are drawn at different chordwise planes. Figures 15, 16, and 17 illustrate TLV of the single rotor (Fig. 15), tandem rotor (Fig. 16), and hybrid

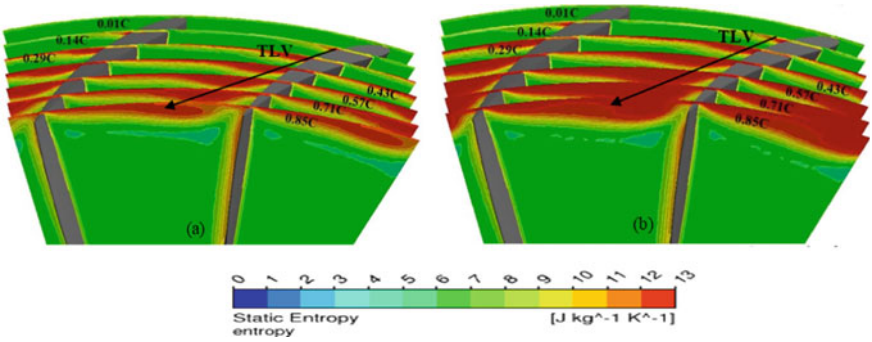

Fig. 15 Entropy contours of single rotor **a** design, **b** off-design condition

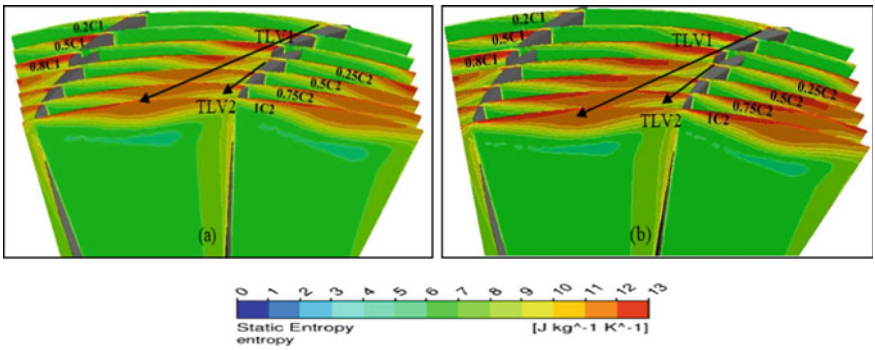

Fig. 16 Entropy contours of tandem rotor **a** design, **b** off-design condition

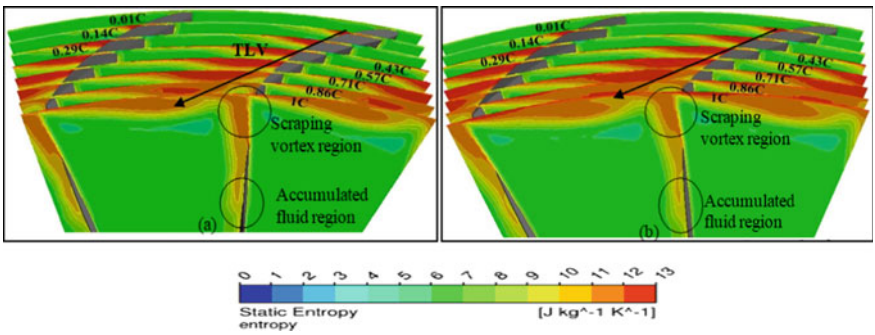

Fig. 17 Entropy contours of hybrid rotor **a** design, **b** off-design condition

rotor (Fig. 17) rotors, respectively, under design and off-design condition. Leakage flow, due to pressure difference between PS and SS, interacts with the main flow and form TLV. Strength of vortex increases as vortex moving toward the mid chord. This vortex migrates toward the PS side of the adjacent blade. Near to TE, TLV stretches and spreads across the passage. For a single rotor, the core of TLV is visible at 14%C. In the case of tandem rotor, two separate TLV can be observed, each associated with FB and AB. The strength of AB TLV is substantially lower than the strength of FB TLV. In tandem, the second TLV starts from AB and interacts with the wakes of FB as well as with the TLV of FB. TLV1 and TLV2 have a different orientation. It appears that TLV2 is more aligned in an axial direction than TLV1. The intensity of TLV1 and TLV2 is lower than the TLV of the single rotor. In the case of the tandem rotor, blade loading is split; hence, two relatively smaller vortices can be seen.

Interestingly, the strength of TLV of the hybrid blade is lower than the strength of single rotor TLV. The entropy region of TLV increases under the off-design condition for all cases except TLV2, which shows a decrement due to reduced tip loading. Stall initiates in the tip region in all rotor cases is due to the TLV effect. Under the off-design condition, entropy generation is highest for the single rotor. In the case of a single rotor and hybrid rotor, scrapping vortex of intensity is visible. The boundary layer of casing rolled up because of the rotating tip and forms scraping vortex which creates high entropy region near to blade SS. For the hybrid rotor, another noticeable entropy zone is visible at or around mid-span blade. However, its strength is substantially lower than the TLV. Further, the strength of TLV and scraping vortex is more at off-design compared to the design point due to higher loading at the tip.

Figures 18, 19, and 20 show contours of Mach number at 98% span of the single rotor, tandem, and hybrid rotor at design and off-design conditions. Low Mach number region indicates blockage created due to TLV. The blockage for the single rotor is considerably higher than the blockage created in other cases. At 98% span, 60% of the blade passage is covered with low velocity fluid. As the strength of TLV increases under off-design condition, blockages region enlarges further and 90% of the blade passage is blocked due to TLV. In the tandem configuration, blockage due to TLV1 and TLV2 merge and form a larger blockage region. It is noteworthy that

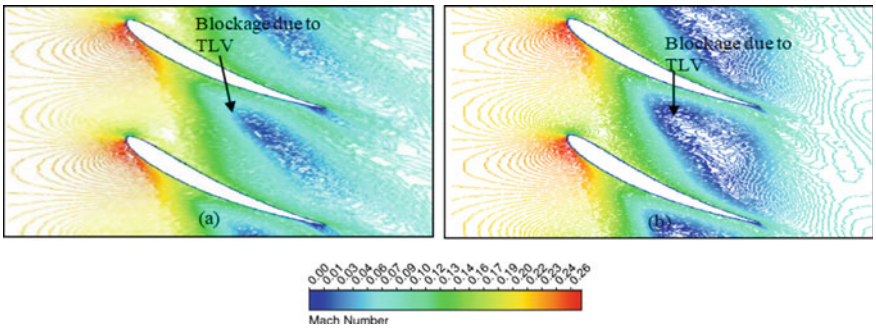

Fig. 18 Mach number contour at 98% span location of single rotor at **a** design, **b** off-design point

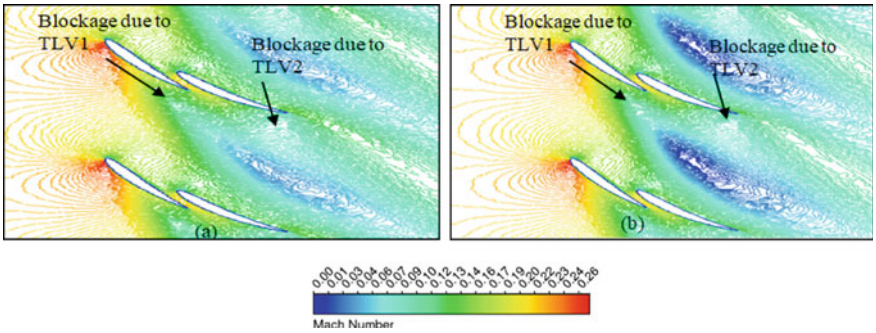

Fig. 19 Mach number contour at 98% span location of tandem rotor at **a** design, **b** off-design point

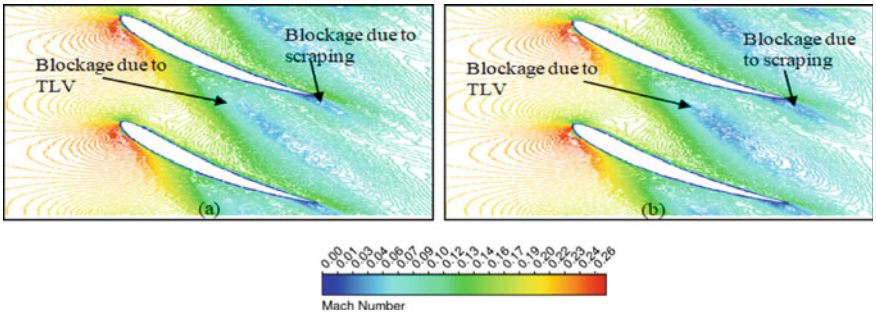

Fig. 20 Mach number contour at 98% span location of part-span tandem rotor at **a** design, **b** off-design point

the flow through gap nozzle reduces the blockage region in the case of the tandem rotor. Scrapping vortex also acts as a source of blockage for the single and hybrid rotor; however, its effect is confined near the trailing edge only.

Static pressure variation from inlet to an outlet under design and off-design condition is plotted in Fig. 21. At LE of the blade due to curvature of the blade, flow accelerates so there is a drop in static pressure at nearly 0.31 streamwise location. Along the blade surface of the rotor, there is a smooth increase in pressure. At 0.34 locations, there is small crust in the tandem case because of LE of AB. There is no large drop in static pressure at LE of AB because of the overlapping region. Under both design and off-design conditions, the tandem rotor shows a higher static pressure rise than the single rotor and hybrid rotor case. The static pressure rise increases at a lower mass flow rate. It is true for all cases. As mass flow rate decreases, blade loading increases due to the higher incidence. The hybrid tandem blade does not show any crust like a tandem rotor. The static pressure rise for hybrid rotor is higher than the single rotor.

Figure 22 shows the surface streamlines over SS of the blades under design condition. Near the hub region, 60% of the blade surface is occupied by radial lines for

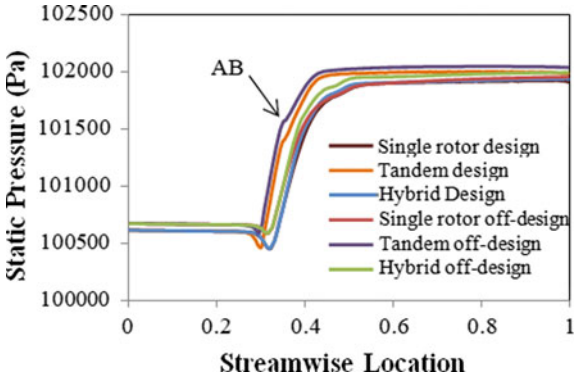

Fig. 21 Comparison of static pressure variation between tandem and hybrid blade

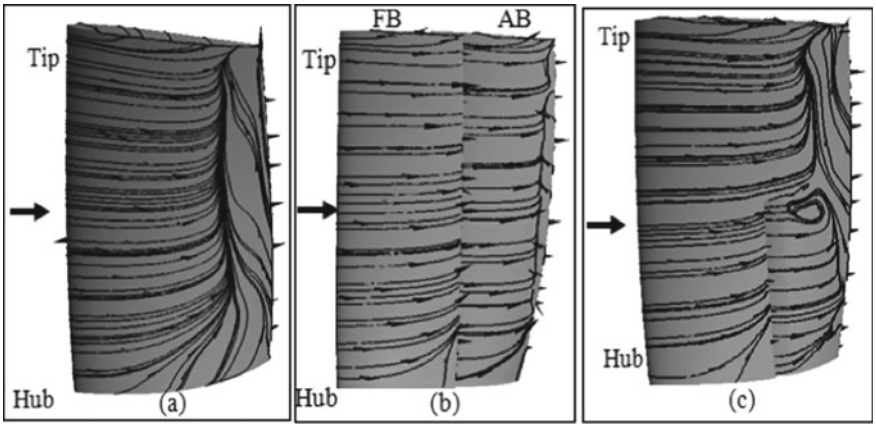

Fig. 22 Skin friction lines at design point over SS **a** single rotor, **b** tandem, **c** hybrid rotor

the single rotor case. At a higher span, flow on SS of single rotor adheres up to 75% of the chord; thereafter, strong radial flow is visible. There are no major changes in surface streamlines at off-design condition (Fig. 23) as these two conditions are close to each other and stall start downstream of the rotor causes no major effect on surface streamlines. In the tandem rotor case, FB's SS is free from any flow reversal. However, small flow separation is visible near the trailing edge portion of AB's SS under design and off-design condition. In case of hybrid rotor, surface streamlines over AB's SS can be interpreted in two distinct regions. The behavior of the surface streamlines up to 50% span can be closely related to the tandem rotor case. Near the mid-span, surface streamlines indicate a formation of strong separation vortex in the case of a hybrid rotor. As explained in the earlier section, near the mid-section, the transformation from two airfoils to single airfoil takes place. At this critical junction, due to the additional boundary layer and inadequate momentum flow, the flow separates from the blade surface at 0.7 chord.

The strength of this vortex increases under the off-design condition.

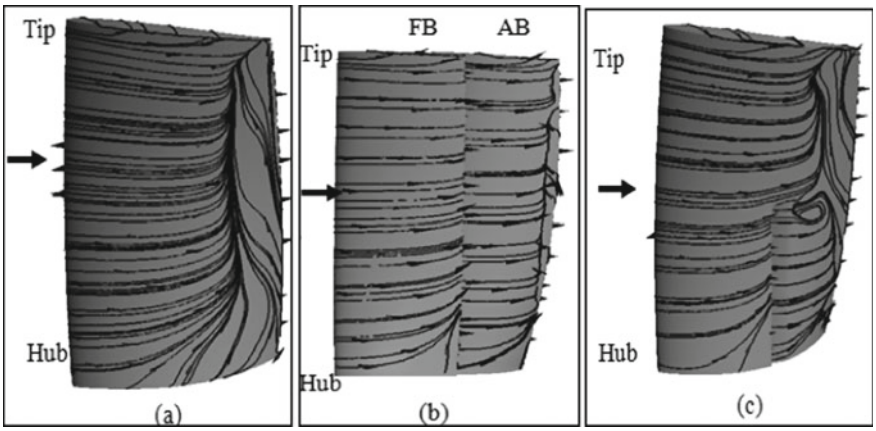

Fig. 23 Skin friction lines at off-design point over SS **a** single rotor, **b** tandem, **c** hybrid

Figure 24 shows the spanwise variation of the total pressure loss coefficient (ω). Due to strong TLV, all cases show higher losses in the tip region (Fig. 24). Moving toward the off-design condition from a design point, losses occur due to TLV further increase. As expected from the earlier discussion, the single rotor experiences a higher loss due to TLV than the tandem rotor and hybrid rotor. After 85% blade span, there is a sharp jump in the loss coefficient for the single rotor. It is important to note that despite having two separate TLV, losses occur due to TLV is much lower in the case of tandem rotor than other cases. It appears that the momentum through gap nozzle promotes the better mixing of TLV with the main flow and subsequently a lower tip leakage loss. The losses of the hybrid blade are higher than the tandem rotor but lower than the single rotor. At a 5% blade span, the tandem rotor and hybrid rotor see a small jump in loss coefficient presumably due to hub corner separation.

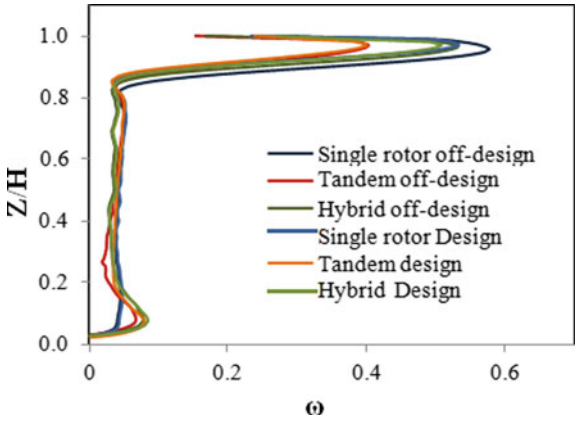

Fig. 24 Total pressure loss coefficient across rotor blade along span

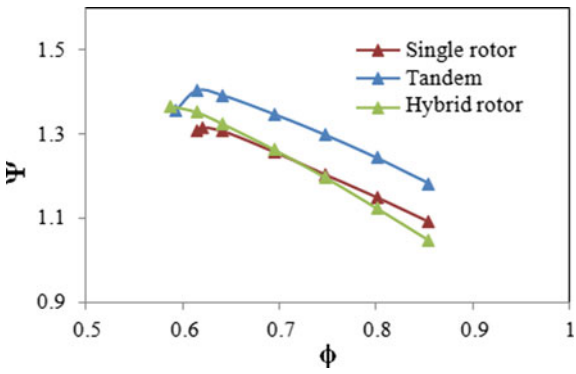

Fig. 25 Stagnation pressure rise coefficient versus flow coefficient

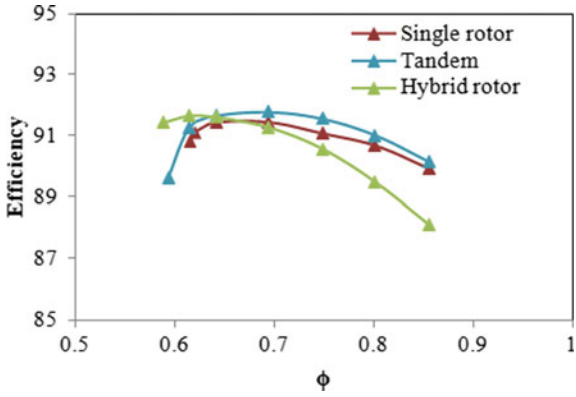

Fig. 26 Isentropic efficiency versus flow coefficient

From a 10% span to an 85% blade span, the loss coefficient is fairly constant and approximately equal for all cases.

Figures 25 and 26 show the performance characteristics of a single rotor, tandem, and hybrid blades. The total pressure rise increases gradually from a higher mass flow rate toward a lower mass flow rate. Near the stall point, the stagnation pressure coefficient drops for the tandem rotor, whereas for other cases experience an abrupt stall. The tandem rotor shows a higher pressure rise as compared to other two cases for the entire range of operation. Under design condition, the tandem rotor has a 5.1% higher total pressure rise than hybrid and a 6.5% higher pressure rise than the single rotor case. This trend is fairly maintained for the entire range of operation. The stall margin for the hybrid rotor is 8.3% while the stall margin for a single rotor and tandem rotor is 4% and 7.5%, respectively. At higher mass, flow rate tandem and single rotors have higher efficiency than hybrid configuration. However, near the stall point, tandem shows a large drop in efficiency. The tandem rotor is able to achieve a higher pressure rise without having any efficiency penalty.

5 Conclusions

The paper discusses the CFD analysis of the single rotor, tandem rotor, and part-span tandem (hybrid) rotor blade. A parallel comparison has been drawn to highlight the benefit and drawbacks of each case. Various parameters like TLV, static pressure variation, Mach number contours, streamlines, and losses have been studied to understand the flow physics with proper reasoning. The error range of the predictions made in the study is in an acceptable range and supported by proper validation and strong theory. The conclusions drawn from the results of low speed analysis are as follows:

- The tandem rotor demonstrates a higher pressure rise as compared to other both cases for the entire range of operation. Under design condition, the tandem rotor has a 5.1% higher total pressure rise than hybrid rotor and a 6.5% higher pressure rise than the single rotor case.
- The stall margin for the hybrid rotor is 8.3% while the stall margin for a single rotor and tandem rotor is 4% and 7.5%, respectively.
- The losses associated with TLV are substantially higher for the single rotor case. The entropy region increases under the off-design condition.
- Despite having two separate TLV, losses occur due to TLV is much lower in case of the tandem rotor than other cases
- In the tandem rotor, the gap nozzle imparts energy to flow on SS of AB. However, near to the hub, the gap nozzle is not working efficiently due to the low momentum of flow and boundary layer effect. The effectiveness of the gap nozzle increases toward the higher span.
- In the case of the hybrid rotor, the nozzle gap is less efficient at the interface zone as compared to the lower spans nozzle gap.
- Blade loading increases from hub to tip. The tandem rotor demonstrates a higher diffusion capability than the other rotors, particularly at a higher span.

References

1. Saha UK, Roy B (1997) Experimental investigations on tandem compressor cascade performance at low speeds. Thermal Fluid Sci 14:263–276
2. Kumar A, Pradeep AM (2018) Optimization of the Gap-nozzle n Tandem Configuration. In: Proceedings of the Asian congress on gas turbines, ACGT2018-TS08
3. McGlumphy J (2008) Numerical investigation of subsonic axial-flow tandem airfoils for a core compressor rotor. PhD diss., Virginia Tech
4. McGlumphy J, Ng W, Wellborn SR, Kempf S (2009) Numerical investigation of tandem airfoils for subsonic axial-flow compressor blades. J Turbomach 131(2):021018
5. Kumar A, Pradeep AM (2018) Performance evaluation of a tandem rotor under design and off-design operation. In: Proceedings of ASME turbo expo: turbomachinery technical conference and exposition, GT2018-75478

6. Guochuan W, Biaonan Z, Guo B (1985) Experimental investigation of tandem blade cascades with double-circular arc profiles. In: Beijing international gas turbine symposium and exposition, ASME, pp V001T02A036–V001T02A036
7. Falla GAC (2004) Numerical investigation of the flow in tandem compressor cascades, Master's thesis, Institute of Thermal Power Plants, Vienna University of Technology, Austria
8. Roy B, Saha UK (1995) High diffusion cascades for axial flow compressor applications. In: Proceedings of 15th Canadian congress of applied mechanics, pp 356–363
9. Bammert K, Beelte H (1980) Investigations of an axial flow compressor with tandem cascades. J Eng Power 102(4):971–977
10. Roy B, Srivastava VP, Mulmule A (2009) Aerodynamic design of Part-Span tandem bladed rotor for low speed axial compressor/fan. In: AIAA applied aerodynamics conference, AIAA 2009–3964
11. Hasegawa H, Akinori M, Shinya S (2003) Development of highly loaded fan with tandem cascade. 41st Aerospace Sci Meet Exh
12. Yoon S, Ajay R, Chaluvadi V, Michelassi V, Mallina R (2019) A passive flow control to mitigate the corner separation in an axial compressor by a slotted rotor blade. In: Proceedings of ASME turbo expo, turbomachinery technical conference and exposition, GT2019